

ARTICLE

Extracellular vesicles facilitate large-scale dynamic exchange of proteins and RNA among cultured Chinese hamster ovary and human cells

Jessica Belliveau^{1,2}  | Eleftherios T. Papoutsakis^{1,2,3} 

¹Department of Chemical and Biomolecular Engineering, University of Delaware, Newark, Delaware, USA

²Delaware Biotechnology Institute, University of Delaware, Newark, Delaware, USA

³Department of Biological Sciences, University of Delaware, Newark, Delaware, USA

Correspondence

Eleftherios T. Papoutsakis, 590 Ave 1743, BPI Bldg., Newark, DE 19713, USA.
Email: epaps@udel.edu

Funding information

Advanced Mammalian Biomanufacturing Innovation Center

Abstract

Cells in culture are viewed as unique individuals in a large population communicating through extracellular molecules and, more recently extracellular vesicles (EVs). Our data here paint a different picture: large-scale exchange of cellular material through EVs. To visualize the dynamic production and cellular uptake of EVs, we used correlative confocal microscopy and scanning electron microscopy, as well as flow cytometry to interrogate labeled cells. Using cells expressing fluorescent proteins (GFP, miRFP703) and cells tagged with protein and RNA dyes, we show that Chinese hamster ovary (CHO) cells dynamically produce and uptake EVs to exchange proteins and RNAs at a large scale. Applying a simple model to our data, we estimate, for the first time, the per cell-specific rates of EV production (68 and 203 microparticles and exosomes, respectively, per day). This EV-mediated massive exchange of cellular material observed in CHO cultures was also observed in cultured human CHR2-288-11 and primary hematopoietic stem and progenitor cells. This study demonstrates an underappreciated massive protein and RNA exchange between cells mediated by EVs spanning cell type, suggesting that the proximity of cells in normal and tumor tissues may also result in prolific exchange of cellular material. This exchange would be expected to homogenize the cell-population cytosol and dynamically regulate cell proliferation and the cellular state.

KEYWORDS

Chinese hamster ovary cells, extracellular vesicles, hematopoietic stem cells, microparticles, protein and RNA exchange

1 | INTRODUCTION

Extracellular vesicles (EVs) are nano- to macro-sized vesicles derived from cytoplasmic or endosomal membranes. EVs are formed by most, if not all, mammalian cell lines and primary cells and constitute a major mechanism of cell-to-cell communication between cells both in vitro and in vivo (Kao & Papoutsakis, 2018, 2019; Raposo & Stoorvogel, 2013). Microparticles (MPs) form from the outward budding of the cytoplasmic membrane and vary in diameter between 100- and 1000-nm. Exosomes, typically 40- to 150-nm in diameter,

are derived from multivesicular endosomes (MVEs) that fuse with the cell membrane, releasing exosomes into the extracellular space (Jiang et al., 2017; Raposo & Stoorvogel, 2013). EVs are highly enriched in small RNAs compared to the parent cell giving EVs the ability to exert regulatory control on target cells. Native EV cargo also includes proteins, mitochondrial DNA, mRNA, lipids, and organelles/organelle fragments (Boudreau et al., 2014; de Jong et al., 2012; Sansone et al., 2017).

Cells use EVs to communicate stress signals, expel toxic by-product accumulation, and send small RNAs to alter the expression

profiles of target cells (de Jong et al., 2012; Han & Rhee, 2018; Njock et al., 2015). There is a large body of literature on the biological effects mediated by EVs in vitro and, increasingly, in vivo (Kao & Papoutsakis, 2019). For example, in in vitro studies, uptake of mesenchymal stem cell derived EVs by breast cancer cell lines has been linked to dedifferentiation of breast cancer cells toward cancer stem cells (Sandiford et al., 2021). Megakaryocyte derived microparticles (MkMPs) have been documented as selectively targeting hematopoietic stem and progenitor cells (HSPCs) (Jiang et al., 2014, 2017), and mesenchymal stem cell derived EVs are selectively taken up by B, NK, and T cells compared to other lymphocyte cells (Di Trapani et al., 2016). Two, among many now, in vivo examples include the impact of human MkMPs in increasing platelet production in a murine model (Escobar et al., 2020) and the use of mesenchymal stem cell derived EVs in clinical trials to improve kidney function in patients with chronic kidney disease (Nassar et al., 2016).

Chinese hamster ovary (CHO) cells are the most widely used cell host in the biopharmaceutical industry for production of therapeutic proteins (Han & Rhee, 2018; Keysberg et al., 2021). CHO cells are grown in suspension cultures in large-scale bioreactors at high cell densities and CHO cell lines are optimized to extend culture lifespan, increase protein production, and limit the accumulation of toxic by-products (Han & Rhee, 2018). Yet very little is known about the biology and impact of EVs on CHO cells in culture. In a recent study (Keysberg et al., 2021), proteomic and small RNA sequencing of CHO EVs harvested from different phases of growth identified differentially expressed proteins and small RNAs. Additionally, the protein and RNA content of the exosomes were compared to the parent cell, identifying proteins and RNAs highly enriched in exosomes, contributing to early understanding of the regulatory effect CHO EVs may have in culture. EVs from CHO cells overexpressing therapeutic enzymes were recently reported to be effective protein delivery vehicles in vitro and in vivo, improving enzyme delivery to hard-to-access organs in traditional enzyme replacement therapies (Seras-Franzoso et al., 2021). Fluorescent studies of CHO EVs from these overexpressing cell lines were observed in vitro to be taken up by primary mouse aortic endothelial cells (Seras-Franzoso et al., 2021). Current literature provides evidence and support for exploring and detailing the dynamic release and uptake of native EVs of CHO and other cells in culture (Han & Rhee, 2018; Keysberg et al., 2021; Seras-Franzoso et al., 2021). Such detailing would shed light to the potential impact of EV exchange between cells on cell fate both in vitro and, by extrapolation, in vivo.

In this study, we aimed to visualize and quantify the extent of EV exchange in culture of CHO cell lines by utilizing correlative confocal and electron microscopy using both fluorescent protein expressing cell lines, lipophilic protein dyes, and fluorescent RNA stains. Correlative confocal and electron microscopy combines the fluorescent capabilities of confocal microscopy to track and quantify individual EVs with the high-resolution imaging of scanning electron microscopy (SEM) to identify individual EVs at the cell surface before EV uptake. In addition to documenting the large-scale exchange of cellular material between CHO cells, extensive levels of EV exchange

were also observed in a human megakaryoblastic cell line (CHRF-288-11) and in primary HSPCs. Based on our findings, we hypothesize that the large-scale exchange of EVs between cells and the associated extensive exchange of proteins, nucleic acids, and lipids, would significantly impact the autonomy of individual cells leading to an ensemble behavior distinct from the behavior of individual cells grown in isolation or in very low culture densities.

2 | MATERIALS AND METHODS

2.1 | Culture of CHO cells, CHRF cells, and human hematopoietic stem and progenitor (CD34⁺) cells (HSPCs)

A recombinant CHO-K1 (Clone A11 from the Vaccine Research Center at the National Institutes of Health) cell line that expresses the anti-HIV VRC01 antibody was cultured in HyClone ActiPro media (Cytiva) supplemented with 6 mM L-glutamine in 125 ml shake flasks at 120 RPM at 37°C in 5% CO₂. RFP CHO-K1 (Innoprot) cells were adapted to HyClone SFM4CHO media (Cytiva) and for suspension growth. GFP CHO-K1 cells were a gift from Dr. Kelvin Lee and were cultured in HyClone SFM4CHO media (Cytiva) in 125 ml shake flasks at 120 RPM at 37°C in 5% CO₂. CHRF-288-11 cells and EmGFP CHRF-288-11 (Fuhrken et al., 2008) were cultured in IMDM supplemented with 10% fetal bovine serum at 37°C in 5% CO₂. HSPCs (CD34⁺ cells) from mobilized peripheral blood were sourced and cultured as previously described (Kao & Papoutsakis, 2018).

2.2 | CHRF cells transiently expressing the fluorescent protein miRFP703

CHRF cells were electroporated following manufacturer protocols for the nucleofector kit V (Lonza) with the pLifeAct-miRFP703 plasmid (Addgene #79993), referred to as miRFP, to express the near-infrared fluorescent protein miRFP703 labeling F-Actin. Briefly, 1×10^6 CHRF cells were electroporated with 4 µg plasmid DNA using U-023 settings (Amaxa) with 2-mm cuvettes.

2.3 | Cell staining using the PKH26 and CFDA-SE, and SYTO RNaselect

Cells and MPs were stained with PKH26 red fluorescent stain (Sigma-Aldrich) following the manufacture protocol to stain proteins in cells and MPs. Isolated cells (180 g, 4 min) and MPs (28,000 g, 30 min) by centrifugation were washed three times in 10% BSA after staining to quench unbound stain. Cells and MPs were resuspended in growth media.

CHO cells stained with 20 mM CFDA-SE dye (Invitrogen,) were incubated at 37°C for 20 min. CHO cells stained with CellTracker

Deep Red were incubated at 37°C for 30 min. Cells were washed three times with PBS before resuspended in growth media.

CHO cells stained with 500 nM SYTO RNASelect green fluorescent cell stain (Molecular Probes) were incubated at 37°C for 20 min according to the manufacture protocol. Cells were washed three times with PBS or growth media before being resuspended in growth media.

2.4 | Setup of cocultures

Cocultures of CHO cells, CHRF cells, and CD34⁺ cells were setup as follows. 2×10^6 CellTracker Deep Red stained CHO cells were cocultured with 2×10^6 CFDA-SE-stained CHO cells. 2×10^6 GFP CHO cells were cocultured with 2×10^6 RFP CHO cells. CHRF cells on Day 3 of culture were electroporated with pLifeAct-miRFP703 plasmid as described above. Electroporated cells recovered for 2 h at 37°C and 5% CO₂. 2×10^6 miRFP CHRF cells were cocultured with 2×10^6 EmGFP CHRF cells. CD34⁺ cells on Day 3 of culture were cocultured at 37°C 5% O₂ with isolated EmGFP CHRF MPs or PKH26 stained CHRF MPs at a ratio of 100:1. CD34⁺ cells on Day 5 of culture followed the same protocol as Day 3, except were cultured at 5% CO₂. All cocultures began in 100 µl for 1 h before expanding the culture volume to 1 ml. Coculture samples were collected at 24 and/or 48 h for confocal microscopy as described below.

Cocultures from stained RNA experiments were setup as follows: 2×10^6 CHO cells stained with SYTO RNASelect were cocultured with 2×10^6 unstained CHO cells beginning in 100 µl for 1 h before expanding the culture volume to 1 ml. Coculture samples were collected for flow cytometry analysis at 0, 1, 2, 4, 6, and 24 h. Three control cocultures were used: a SYTO RNASelect stained culture, an unstained culture, and an unstained culture grown in the final-wash supernatant from the stained cultures. This last control was to ascertain that no SYTO RNASelect dye could remain in the medium that could stain unstained cells.

2.5 | Isolation of extracellular vesicles

CHO EVs were isolated from culture media with differential ultracentrifugation from Day 3 CHO cultures. Cells were removed from the media by centrifugation at 180 g for 4 min. Cellular debris and apoptotic bodies were removed by centrifugation at 2000 g for 10 min. CHO MPs were isolated at 28,000 g for 30 min by ultracentrifugation (Beckman Coulter Optima LE-80K Ultracentrifugation, SW-28 rotor) and concentrated at 28,000 g for 30 min with the Beckman Coulter Optima MAX Ultracentrifuge (TLA-55 rotor). CHO MPs were resuspended in growth media and used immediately or stored at 4°C overnight.

CHO exosomes were isolated from the supernatant after isolating CHO-MPs by filtering (0.22 µm) and centrifuged at 100,000 g for 90 min (SW-28 rotor, Beckman Coulter Optima LE-80K). Then, CHO exosomes were concentrated with the Beckman Coulter Optima MAX Ultracentrifuge (TLA-55 rotor) at 100,000 g for 90 min. CHO exosomes were resuspended in growth media and used immediately or stored at 4°C overnight.

2.6 | Zeta potential and nanoparticle tracking analysis (NTA) of EVs

CHO EVs were counted with Nanoparticle Tracking Analysis (NanoSight NS300, Malvern Panalytical) at a 200-fold dilution in filtered PBS. Five microliters of isolated CHO MPs or CHO exosomes were suspended in 1 ml of PBS and the zeta potential was measured on the Litesizer 500 (Anton Paar) at 25°C.

2.7 | Quantitation of EV accumulation

The accumulation (dE/dt) of CHO MPs and exosomes was determined by finding the difference in MP and exosome concentrations between sequential days as determined by NTA. A polynomial curve was fitted to the temporal MP and exosome accumulation data to determine an equation for describing the temporal MP and exosome accumulation. Due to the large spread in Day 6 MP counts amongst the three biological replicates, Day 6 MP counts were excluded from the fitted line calculation. An exponential curve was fitted to the temporal cell concentration data of Days 1–5 of culture (exponential growth) to determine an equation for describing cell concentration.

2.8 | Flow cytometric analysis of exosomes and microparticles

Characteristic protein surface markers of exosomes were evaluated on CHO exosomes and microparticles by flow cytometry. Following manufacturer protocols, Dynabeads Protein G Immunoprecipitation Beads (Invitrogen) were coated in exosome targeting capture antibodies, CD63 (SCBT #55051), CD81 (cell signaling #10037 S), TSG101 (SCBT #7964), and Annexin A1 (cell signaling #3299 S). Exosomes and MPs were captured on the antibody-coated beads overnight with gentle shaking at 4°C. Bead-bound EVs were isolated with a magnetic separator and detected with the same capture antibodies (CD63, CD81, TSG101, and Annexin A1) and stained with a fluorescently conjugated secondary antibody for flow cytometry. Control samples for flow cytometry analysis included antibody-coated beads to control for the fluorescence of the beads. Additionally, antibody-coated beads were treated with the secondary antibody to control for fluorescent antibodies binding to the beads and for the secondary antibody detecting free capture antibody on the bead surface.

2.9 | EM of CHO cells and CHO EVs (SEM and TEM)

CHO cells and CHO EVs for SEM were fixed in 4% EM grade glutaraldehyde overnight on poly-L-lysine coated glass coverslips (Fisher Scientific). Samples were processed for SEM imaging by treating the samples to 1% osmium tetroxide for 1 h, three washes with nanopure

water, and a series of ethanol dehydration steps (25%, 50%, 75%, 95%, 100%, 100% ethanol). The dehydration process was finished with a CO₂ critical point drier (Autosamdri 815 A, Tousimis) and samples were coated with 5 nm platinum before SEM (Hitachi S4700 and Apreo VolumeScope) imaging.

CHO EVs for TEM imaging were placed on 400 mesh carbon-coated copper grids (Electron Microscopy Sciences) and stained with uranyl acetate for negative staining. EV diameters were measured in ImageJ.

Coculture samples in correlative confocal microscopy and SEM microscopy experiments were seeded onto poly-L-lysine coated coverslips or gridded wells (Ibidi) for 10 min, fixed with 4% PFA for 10 min, and washed three times with PBS. CD34⁺ cell cocultures were stained with PKH26 (before seeding) or Alexa Fluor 647 Phalloidin (after fixation) to visualize the cell membrane. Coculture samples on coverslips were mounted onto glass slides with SlowFade Diamond Antifade Mountant with DAPI (Invitrogen) for imaging. Cells on gridded wells were stored in PBS for imaging.

In correlative confocal microscopy and SEM studies, after CHO cocultures were imaged with confocal microscopy, samples were processed for SEM imaging as described above.

2.10 | Image processing

Post-microscopy analysis was done in Zen Black (Zeiss) for confocal images and Icy (De Chaumont et al., 2012) for correlative processing using the EC-CLEM plug-in (Paul-Gilloteaux et al., 2017). Widefield images with surrounding cells were used as regions of interest (ROIs) to determine the 2D transformation matrix to account for the difference in sample orientation between the confocal microscope and SEM as well as the inversion of images due to the differences in imaging software. The 2D transformation was applied to maximum intensity images of individual cells to align the confocal images to the SEM images. To account for the three-dimensionality of the SEM images relative to the two-dimensionality of the confocal images, ROIs were determined on the perimeter of the maximum intensity projection (MIP) image to “wrap” the confocal image onto the SEM image.

3 | RESULTS

3.1 | Characterization of CHO EVs

Characterization of CHO EVs harvested from CHO cultures via differential ultracentrifugation (Figure 1a) included size distribution, zeta potential, surface markers, and surface morphology.

To understand the relationship between the accumulation of MPs and exosomes in the media and culture growth phase, three biological replicates of 10 cultures with the same seeding density and growing conditions were set up. For each biological replicate, one culture was harvested daily to measure cell concentrations and

isolate EVs for quantification via nanoparticle tracking analysis (NTA). In Figure 1b, the number of MPs in the media increased from 5.3×10^6 on Day 1 of culture to 1.9×10^{11} on Day 10. The number of exosomes in the media increased from 1.8×10^9 on Day 1 of culture to 1.9×10^{11} on Day 10. Only on Days 2 and 4 was there significantly more exosomes in culture than MPs. The accumulation (dE/dt) of MPs and exosomes in the media over the course of culture were fitted to polynomial curves (Figure 1c) to calculate the rate of EV accumulation. The two curves (Figure 1c) are almost linear with time. Counting the number of MPs and exosomes in the media at any given time does not reflect the absolute number of EVs being generated by the cultured cells as EVs that are taken up by other cells (as detailed below) cannot be accounted for. Thus, the total number of EVs produced per cell is greater than what we measure.

A simple model of EV production and consumption was used to estimate the rate of EV generation and EV uptake. EV accumulation (dE/dt) in the media is equal to the difference between the rates of EV generation and the rate of EV uptake. The rate of EV generation is proportional to the cell concentration (C) with a proportionality constant of k_1 . EV uptake is proportional to the collision probability between a cell and an EV and is represented by k_2CE , where E is the EV (MP or exosome) concentration. It assumes that one collision event between an EV and a cell will not affect the collision probability of the same cell with other EVs, and that all collision events have the same probability of resulting in EV uptake by the cell. Thus,

$$\frac{dE}{dt} = k_1C - k_2CE, \quad (1)$$

k_1 represents the number of EV produced per cell per unit time. The rate of EV uptake per cell then is k_2E and is increasing with time as E is increasing with time. On a per cell basis, this equation can be written as:

$$\frac{1}{C} \frac{dE}{dt} = k_1 - k_2E. \quad (2)$$

Thus, the specific (per cell) rate of EV accumulation is equal to the specific rate of EV formation (k_1) minus the specific rate of EV uptake (k_2E). We note that after Day 1, dE/dt is a positive number until about Day 7 of the culture as shown in Figure 1c. Although in Figure 1c we fit the data with a simple curve as discussed above, the plateauing of the EV number versus t curve of Figure 1b shows that the net accumulation rate (dE/dt) becomes eventually zero, and for exosomes slightly negative after Day 7. This means that the rate of formation is higher than the rate of uptake and that the two rates become approximately equal to each other after about Day 8. In a first approximation estimate, the two rate constants (k_1 , k_2) were assumed constant for the whole duration of the culture. Because dE/dt is a positive number throughout the culture:

$$k_1 \geq k_2C \text{ or } (k_1/k_2) \geq E$$

Because E is a very large and increasing number and k_2 a very small number, estimation of k_1 and k_2 from plotting the data is very difficult. To resolve this difficulty, we hypothesized that EV

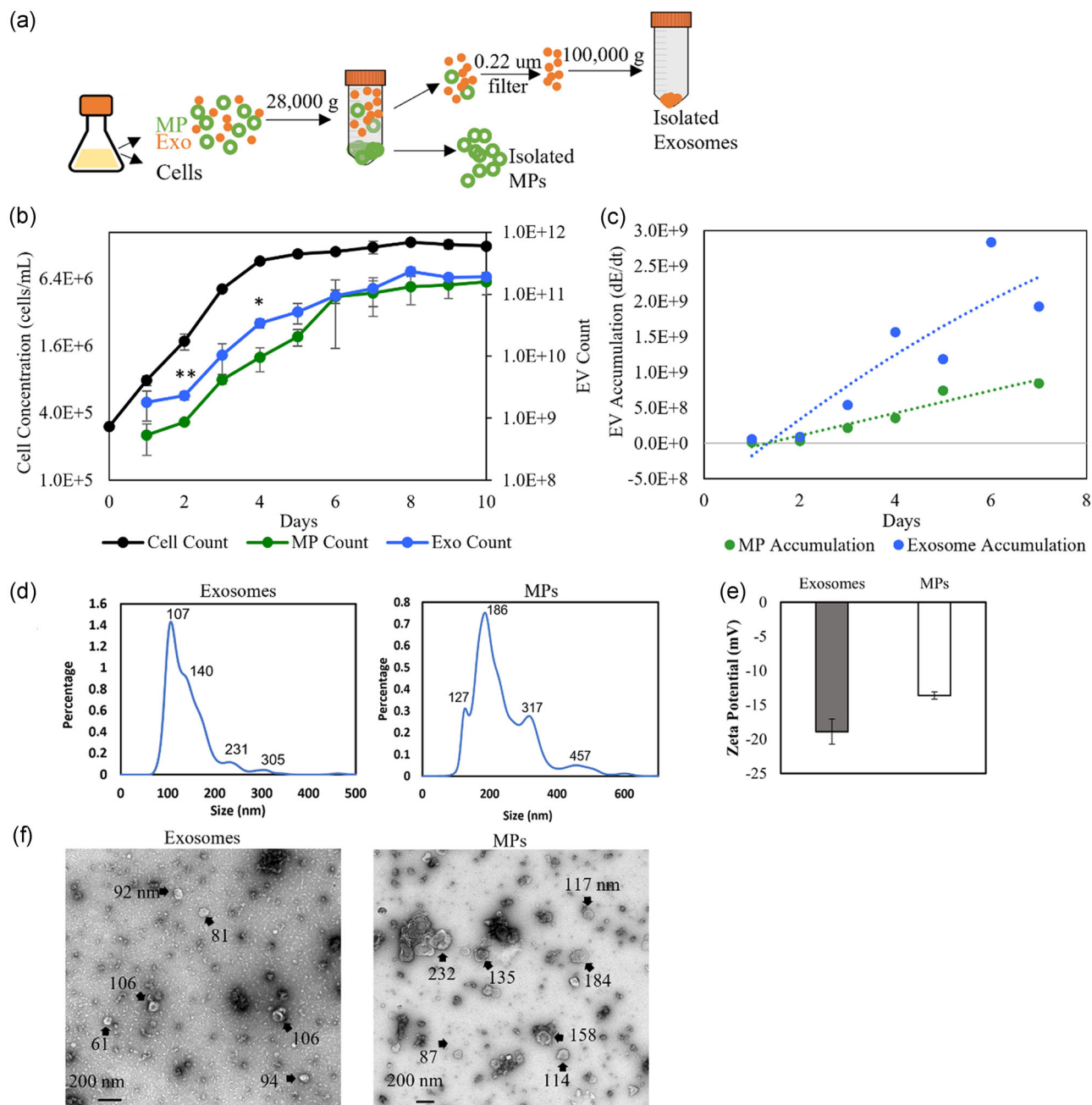


FIGURE 1 Characterization of Chinese hamster ovary (CHO) extracellular vesicle (EVs). (a) Overview of isolation of CHO exosomes and microparticles (MPs) by differential ultracentrifugation. (b) CHO cell (black), microparticle (green), and exosome (blue) concentration of cultures over 10 days of culture from a starting seed density of 0.4×10^6 cells/ml in 15 ml cultures (three biological replicates). Microparticle and exosome concentrations, measured by nanoparticle tracking analysis (NTA) were significantly different on Days 2 and 4 of culture. (c) MP and exosome accumulation over seven days of culture. Polynomial curves were fitted to describe EV accumulation. Day 6 MP counts were not included. The fitted equations (t in days) to describe MP and exosome accumulation were:

$$\frac{dE_{MP}}{dt} = -1.35 \times 10^5 t^2 + 1.59 \times 10^8 t - 2.09 \times 10^8 \text{ and } \frac{dE_{Exo}}{dt} = -1.82 \times 10^7 t^2 + 5.65 \times 10^8 t - 7.22 \times 10^8$$

(d) CHO exosome (left) and MP (right) size characterized by NTA. The mode size of exosomes was 107 nm and the mode size of microparticles was 186 nm. (e) The zeta potential of CHO exosomes was -13.5 mV and MPs was -13.6 mV. (f) Size characterization and membrane integrity after ultracentrifugation were observed by TEM of CHO exosomes (left) and MPs (right). Error bars represent the standard deviation from the average of three biological replicates with $*p < 0.1$ and $**p < 0.05$

generation is the dominant term in Equation 1, at the early days at least when both C and E have lower values. This was confirmed by the reasonable fit of the data at the early time points with a straight line on the dE/dt versus C plot (Figure S1b,c). From the slopes of these plots (Figure 1b,c) we can estimate the k_1 values. We note that the hypothesis of linearity will result in a small overestimation of the specific rate of EV formation (k_1). On a per cell basis, in the first 4 days of culture, approximately 68 MPs (k_{1MP} for MPs) were produced per day. On a per cell basis, in the first 4 days of culture, approximately 203 exosomes (k_{1Exo} for exosomes) were produced per day. The accuracy of the data do not permit even an approximate value for k_2 and thus of the rate of EV uptake per cell ($=k_2E$) changes with time as E increases. From the data of Figure 1, all we can say is that that $k_2E \leq k_1$ until about Day 8 for exosomes and a little longer for MPs. We discuss below how k_2 can be estimated.

Measured by NTA, the mode, or highest frequency, size of CHO MPs and exosomes is 186 and 107 nm, respectively (Figure 1d). The zeta potential, approximating the surface charge of the EVs (Midekessa et al., 2020), of the CHO MPs and exosomes was -13.6 and -13.5 mV, respectively (Figure 1e). Reported exosome values range from -10.3 to -55 mV (Han & Rhee, 2018; Kesimer & Gupta, 2015; Midekessa et al., 2020; Sokolova et al., 2011). SEM and transmission electron microscopy (TEM), was used to examine the surface morphology of CHO EVs (Figure 1f). The diameter of the CHO MPs and CHO exosomes imaged with TEM were measured in ImageJ. The measured EV diameters in the TEM samples were representative of the diameter size distribution measured by NTA. Additionally, EV morphology observed with TEM was similar to other reported CHO EV samples

isolated via differential ultracentrifugation (Keysberg et al., 2021). SEM of CHO cells (Figure 2) shows the surface of CHO cells have small, round, MP-like protrusions that were approximately 0.64 - to 1.4 - μm in diameter. We hypothesize that some of the protrusions at the cell surface are CHO MPs being produced, and some are CHO EVs the cell is taking up from the culture. This is pursued further below.

We examined a recently proposed surface protein marker of microparticles, Annexin A1 (Jeppesen et al., 2019), and commonly reported surface protein markers of exosomes, CD63, TSG101, CD81 (Han & Rhee, 2018; Seras-Franzoso et al., 2021), to characterize the different isolated EV populations via differential ultracentrifugation (Figure 3). Protein G coated Dynabeads were functionalized with one antibody targeting an EV surface marker (Annexin A1, CD63, TSG101, or CD81). The presence of the EV surface markers on isolated MPs and exosomes was determined via flow cytometry by the binding of the EV to the antibody-coated beads and staining with the corresponding antibodies (Garcia-Contreras et al., 2017). The mean fluorescent intensity (MFI) of the MP and exosome samples captured on Annexin A1, CD63, TSG101, and CD81 antibody-coated beads was compared to the secondary control ($n=3$). Antibody-coated beads were incubated with the secondary antibody without exosomes or MPs as a control for fluorescence of the secondary antibody binding directly to the bead. The secondary control determined the baseline for the MFI due to the secondary antibody binding directly to the bead or to the primary antibodies on the bead surface. Exosomes (Figure 3a,b) had high expression of the surface markers Annexin A1 and CD81, while CD63 and TSG101 were

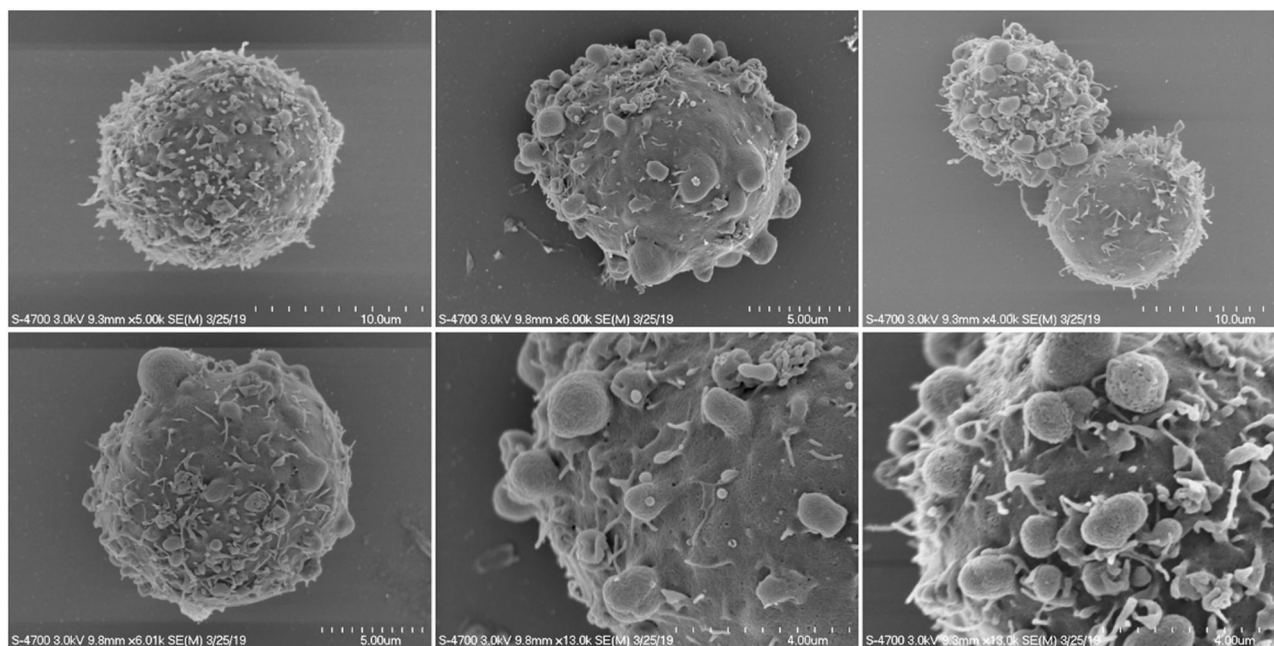


FIGURE 2 Electron microscopy of Chinese hamster ovary (CHO) cells. Scanning electron microscopy images of CHO cells in culture with extracellular vesicle (EV)-like structures at the cell surface. Under normal culture conditions, cells appear with numerous EV-like structures and cells also appear without any EV-like structures at the surface

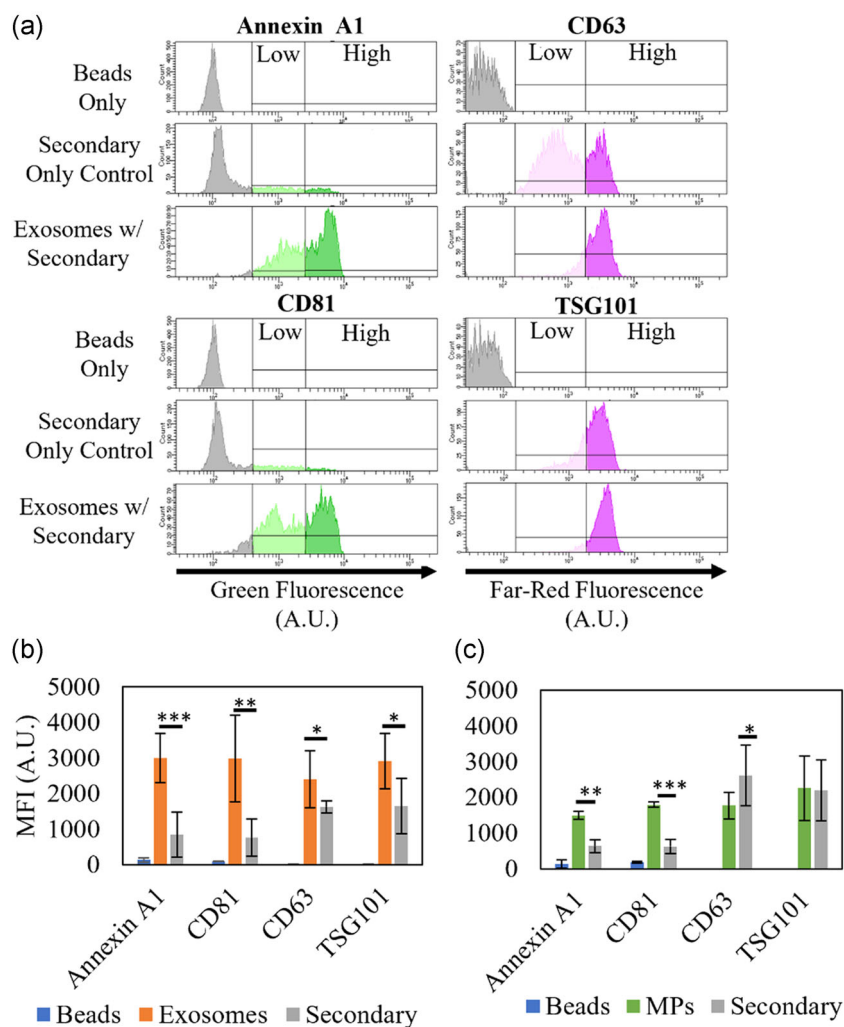


FIGURE 3 Extracellular (EV) vesicle surface protein characterization using flow cytometry. Chinese hamster ovary (CHO) exosome and MPs were isolated and captured on antibody-coated capture beads to detect a reported microparticle marker (Annexin A1) and exosome markers (CD63, CD81, and TSG101) using flow cytometry. (a) Histograms and (b) mean fluorescent intensity (MFI) of captured CHO exosomes demonstrate the shift in fluorescent intensity due to the presence of surface proteins on the exosomes bound to the capture beads compared to the negative control, capture beads only, and secondary antibody control, capture beads incubated with the fluorescent (AlexaFluor 488 or AlexaFluor 647) secondary antibody. Exosome captured samples display higher levels of fluorescence compared to the low levels in the secondary only control indicating the presence and abundance of surface markers. CHO exosomes display all four surface proteins, Annexin A1, CD81, CD63, and TSG101 at a MFI significantly greater than both control conditions. (c) CHO MPs display Annexin A1 and CD81 at a MFI significantly greater than both controls, but do not display the surface proteins CD63 or TSG101 indicating differences in surface protein composition between CHO MPs and exosomes. Error bars represent the standard deviation of three replicates with * $p < 0.1$, ** $p < 0.05$, and *** $p < 0.01$

detected on the exosomes at a lower abundance as determined by the differences in MFI. CHO EVs have been reported in other studies to be high in CD81 expression and lower in TSG101 expression (Han & Rhee, 2018; Keysberg et al., 2021). MPs (Figure 3c) had high expression of the surface markers Annexin A1 and CD81 compared to the secondary control. CD63 and TSG101 were not detected on MPs indicating EV isolation via differential ultracentrifugation isolated two different EV populations. Additionally, Annexin A1 does not appear to be a microparticle-specific marker for CHO MPs as it was detected in both the exosome and MP populations.

3.2 | EVs mediate profound dynamic exchange of proteins and RNA between CHO cells

EVs are packaged with RNAs and proteins from the parent cell and are released into the culture. Here, we examined the extent to which CHO cells exchange cellular material by releasing and taking up EVs. Correlative confocal and SEM, as well as flow cytometry, were used to visualize and quantify the extent of material exchange through fluorescently stained total cellular proteins, cell lines producing fluorescent proteins, or fluorescently stained RNA. Correlative confocal microscopy and SEM

combine fluorescent imaging with confocal microscopy and high-resolution imaging via SEM. The combination of these two microscopy methods makes it possible to identify individual EVs (produced by other cells in the culture) on the surface of individual CHO cells as part of the uptake process. Visualizing uptake of CHO EVs in culture builds upon our understanding of EV uptake by cells and the extent to which proteins and RNAs are being shared between cells. Additionally, MIP images via confocal microscopy alone enables the visualization of the total number of EVs taken up by a CHO cell while still largely intact in the cell at the time of sampling. This allows for the assessment of the total

amount of cellular material being shared amongst cells in culture at a given timepoint.

3.2.1 | Cell staining using viable protein dyes

CHO cells stained with CellTracker Deep Red, a far-red fluorescent dye, and CFDA-SE, a green-fluorescent dye, were cocultured for 24 h. The extent of EV exchange between Deep Red stained and CFDA-SE-stained cells was measured with confocal microscopy and correlative confocal/SEM (Figure 4).

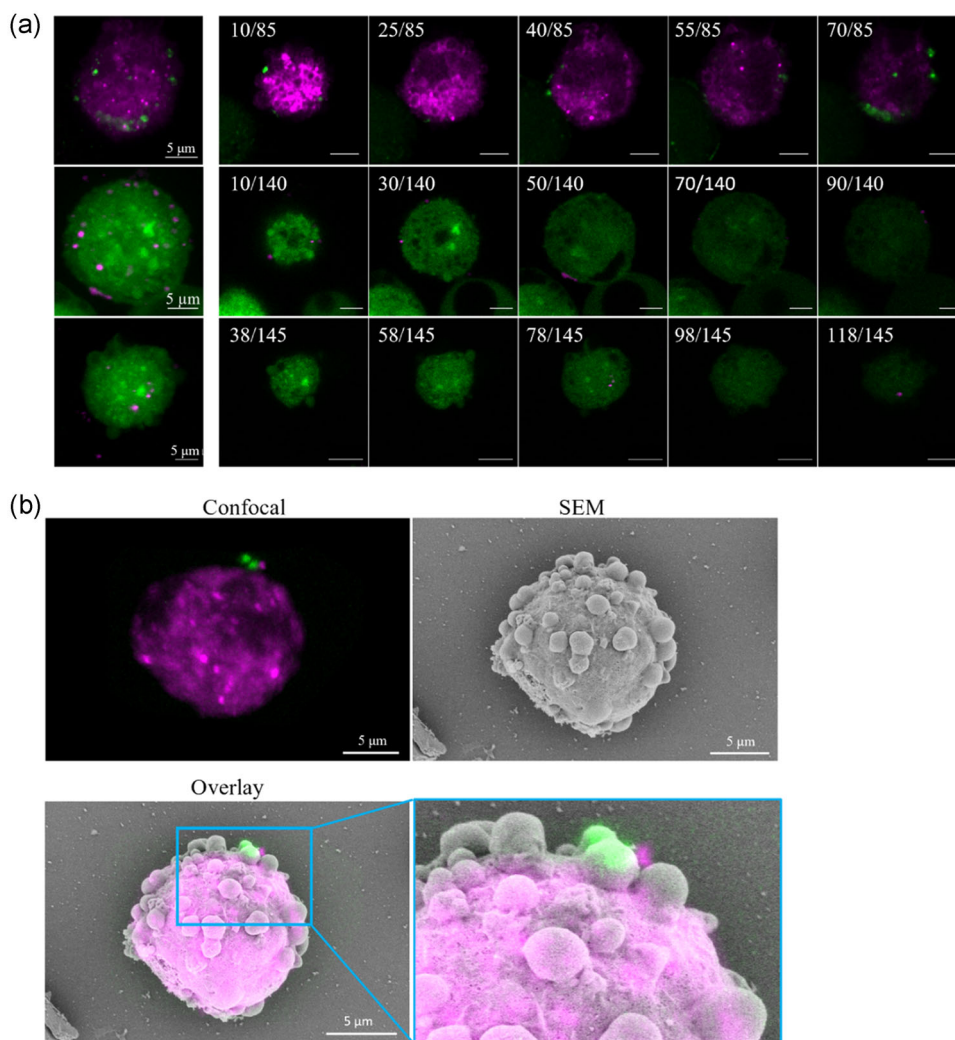


FIGURE 4 Visualizing the extent of Chinese hamster ovary (CHO) extracellular vesicle (EV) exchange between cells using protein stains and correlative fluorescence-SEM microscopy. CFDA-SE stained (green) CHO cells (2×10^6 cells) and CellTracker Deep Red (magenta) CHO cells (2×10^6 cells) were cocultured in 100 μ l growth media for the first hour to enhance the contact between cells and EVs. After the first hour, the coculture was diluted with growth media to 1 ml for 24 h. At $t = 24$ h, cells were assessed for EV exchange via confocal microscopy and scanning electron microscopy (SEM). (a) Confocal z-stack images of cells in the coculture visualize the exchange of fluorescent protein material between cells in culture via EVs. Maximum projection intensity images of three example cells (far left images) capture all z-stack images at once and qualitatively evaluate the amount of EV exchange at 24 h of coculture. Individual z-stack images of the example cells (right images) at incremental changes in the z-direction (where 10/85 represents the tenth image in the z-plane out of 85) show where the EV is located in the target cell. (b) Correlative SEM and confocal microscopy identified individual CFDA-SE CHO EV uptake events by a CellTracker DeepRed cell. Two individual CFDA-SE EVs are observed at the cell surface before EV uptake. ICY EC-CLEM image analysis software was used to rotate and transform the confocal images to be mapped onto the SEM image and overlay the confocal and SEM image

From the coculture at 24 h, three representative cells are shown in Figure 4a as MIP images to visualize the entire cell in a single image and individual z-plane images to give context as to the relative location of the EV in the cell. In these snapshots, Deep red stained CHO cells contain EVs produced by CFDA-SE stained cells and CFDA-SE stained CHO cells contain EVs produced by Deep Red stained cells. MIP images reveal that the cells in coculture take up multiple EVs at a given time. The majority of EVs we detected were located at the cell periphery suggesting these are recent uptake events.

Additionally, the EV-like structures observed at the cell surface in Figure 2 were seen in the correlative confocal/SEM images with EV-like structures containing stained protein in Figure 4b. Correlative confocal/SEM was used to observe specific uptake events on the surface of target CHO cells by identifying fluorescent CHO EVs at the cell surface with confocal microscopy and imaging the same cell with SEM to visualize the CHO EV interacting with the cell surface. MIP images from confocal microscopy were rotated and transformed to match the orientation and size of the SEM images utilizing the location of neighboring cells to calculate differences in orientation and size in the imaging software ICY and extension EC-CLEM. In Figure 4b, a Deep Red stained CHO cell was observed taking up two EVs produced by a CFDA-SE cell through membrane fusion.

Decreases in fluorescent intensity due to cell division and dilution of protein stain was a major challenge in tracking the true extent of EV exchange via confocal fluorescence microscopy and even more so via flow cytometry. In stained cells, evaluating the shift in increasing fluorescent intensity as EVs are taken up over the culture lifespan competes with the decreasing shift in fluorescence of cells. Additionally, we hypothesize that after an EV is taken up and the cargo is released into the cell, the stained proteins become too dilute to detect. Thus, while fluorescent protein stains are a good tool for understanding EV release and uptake during cell culture, to better understand the extent of EV exchange, CHO cell lines expressing GFP and RFP were utilized. Fluorescent proteins stably expressed in CHO cells do not decrease in fluorescent intensity due to cell growth like cultures using staining with fluorescent dyes, and we thus expected an improved assessment of EV exchange between cells.

3.2.2 | Use of fluorescent-protein expressing CHO cells lines

Cocultures of GFP expressing CHO cells and RFP expressing CHO cells demonstrate the widespread exchange of CHO EVs in culture and enable quantification of the EV-exchange process. CHO EV exchange via fluorescent proteins was evaluated with confocal microscopy and correlative confocal/SEM at 24 h of coculture. (Figure 5). Representative images from the coculture at 24 h in Figure 5a capture the exchange of GFP RFP between cells via EVs. MIP images of entire cells from the coculture demonstrate the total amount of fluorescent protein exchange with the observed exchange similar to the fluorescent protein stain cocultures.

Correlative confocal/SEM reveal individual EV uptake events at the cell surface (Figure 5b,c). Figure 5b shows the confocal and SEM images of a GFP CHO cell with RFP CHO EVs and the overlay of the confocal images with the SEM image. Correlating the confocal images with the SEM image enabled the identification of three RFP CHO EVs at the cell surface (Figure 5c). SEM images capture the GFP CHO cell microvilli interacting with the RFP CHO EV before uptake. Interactions between EVs and microvilli in the uptake process was also observed by Jiang et al. (2017) and suggested that early interactions between EVs and microvilli are important for EV uptake.

CHO EV exchange was evaluated with confocal microscopy by observing the transfer of RFP and GFP in individual cells in a wide-field image at 24 h of coculture (Figure 6). In a representative wide-field image with fifteen individual CHO cells, every cell had taken up fluorescent CHO EVs, indicating that CHO EV exchange in CHO cultures is widespread. MIP confocal microscopy images (Figure 6) demonstrated the range of EV uptake by CHO cells, with some cells containing one or two EVs detectable at a given timepoint and others containing upwards of fifteen EVs. As EVs are taken up, the fluorescent proteins within the EVs are released into the cells leading to a decrease in EV-fluorescence intensity and reduced detection.

Although confocal microscopy using RFP and GFP revealed that all cells had taken up EVs from cells expressing a different fluorescent protein, upon uptake, the fluorescence of EVs labeled with a fluorescent protein (which is small fraction of the total cell content) is quickly diluted inside the cells. Thus, even with RFP and GFP expressing cells, we still capture only a small fraction of the likely extent of EV exchange using confocal microscopy and even less so using flow cytometry (data not shown). As noted, confocal microscopy mostly captures labeled EVs on or near the cellular membrane of CHO cells, thus suggesting that the combination of fluorescent-protein dilution in the cytoplasm and the fluorescence quenching effect of the cellular membrane prevents a more accurate assessment of the impact of EV exchange between cells. Thus, we sought a different, stronger fluorescent probe to label a larger fraction—compared to a single fluorescent protein—of the cell content.

3.3 | Staining cellular RNA via the SYTO RNASelect dye enables Flow-Cytometric demonstration of the EV-mediated massive exchange of cellular material between cells

To overcome the limitation of using protein stains or fluorescent proteins for flow-cytometric analysis of cellular-material exchange between cells through EVs, we used an RNA specific fluorescent stain. The SYTO RNASelect dye is specific for RNA detection and only fluoresces green when bound to an RNA molecule. This dye has proven exceptionally robust and specific for labeling cells, and has been successfully used for flow cytometric analysis of microbial cells (Charubin et al., 2020), which is a more challenging task compared to analysis of mammalian cells. Cocultures were designed with half of the CHO cells stained with the SYTO RNASelect dye and half of the

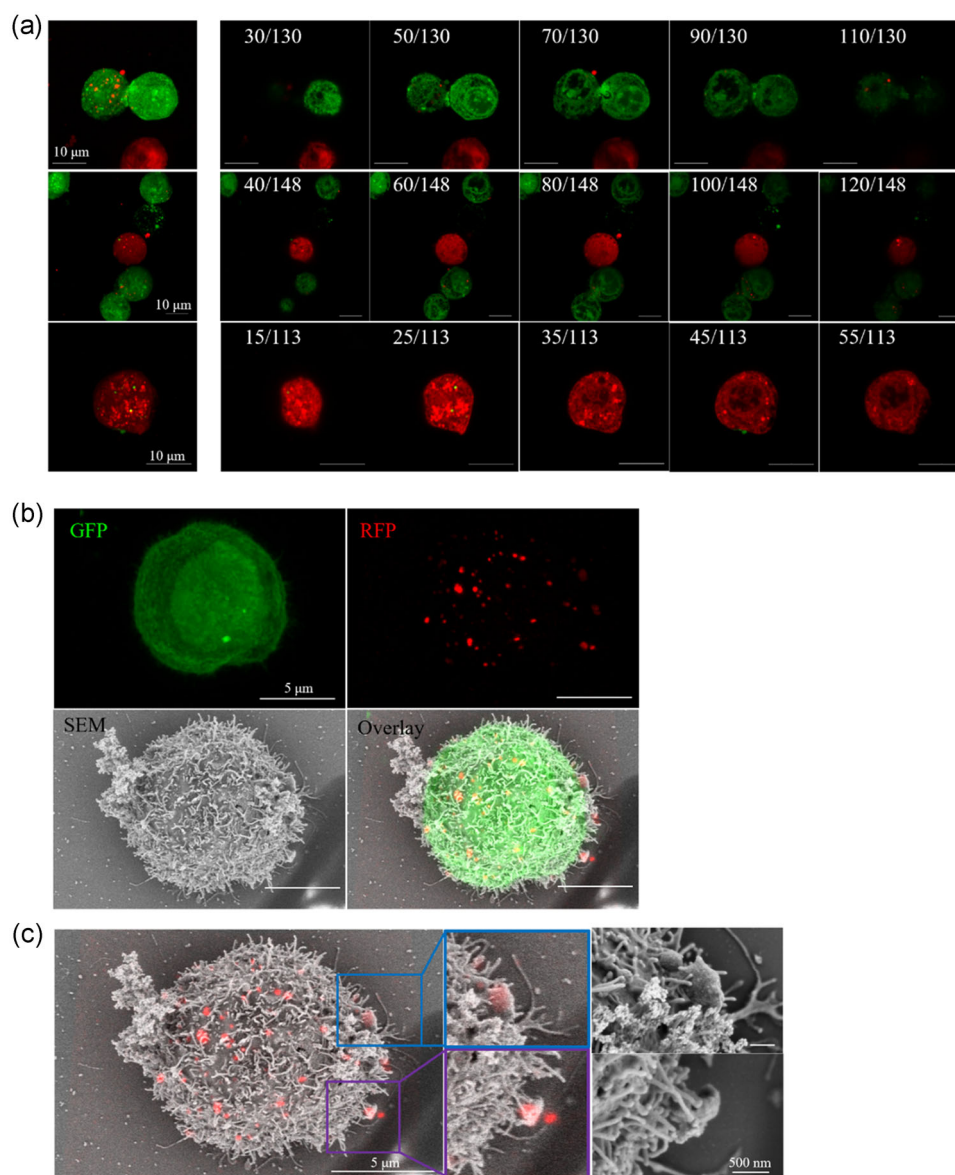


FIGURE 5 Visualizing the extent of GFP/RFP Chinese hamster ovary (CHO) extracellular vesicles (EVs) exchange between cells using correlative microscopy. GFP expressing (green) CHO (2×10^6 cells) and RFP expressing (red) CHO (2×10^6 cells) cells were cocultured in 100 μ l growth media for the first hour to enhance the contact between cells and EVs. After the first hour, the coculture was diluted with growth media to 1 ml for 24 h. At $t = 24$ h, cells were assessed for EV exchange via correlative confocal microscopy and SEM. (a) Confocal microscopy z-stack images of cells in the coculture demonstrate the exchange of the fluorescent proteins GFP and RFP via EVs. Maximum projection intensity images of three example cells (far left images) capture all z-stack images at once and qualitatively evaluate the amount of EV exchange at 24 h of coculture. Individual z-stack images of the example cells (right images) at incremental changes in the z-direction (where 30/130 represents the 30th image in the z-plane out of 130) show where the EV is located in the target cell. (b) Correlative confocal microscopy (GFP and RFP separated into individual channels) and SEM of RFP CHO EVs taken up by a GFP expressing cell. Confocal microscopy demonstrates the massive amount of protein exchanged between cells via EVs. Confocal images are maximum intensity projections, where all z-planes are overlaid and displayed in a single image. ICY EC-CLEM image analysis software was used to rotate and transform the confocal images to be mapped onto the SEM image and overlay the confocal and SEM image. (c) Merged SEM and confocal microscopy (RFP channel only) identify several RFP EVs at the cell surface and high-resolution SEM images of the identified EVs. High-resolution SEM images reveal EVs are interacting with microvilli on the cell membrane potentially as an early cellular mechanism to initiate EV uptake

CHO cells unstained. Three biological replicates of cocultures were examined flow cytometrically over the course of 24 h to determine the fraction of cells displaying SYTO RNaselect fluorescence. At the start of the coculture (Figure 7a), 51% of the cells displayed SYTO

RNaselect fluorescence and 49% of the cells did not. At 6 h and 24 h of coculture, 75% and 98% of cells displayed SYTO RNaselect fluorescence, respectively. Figure 7a captures the shift in green fluorescent intensity of one of the three coculture biological

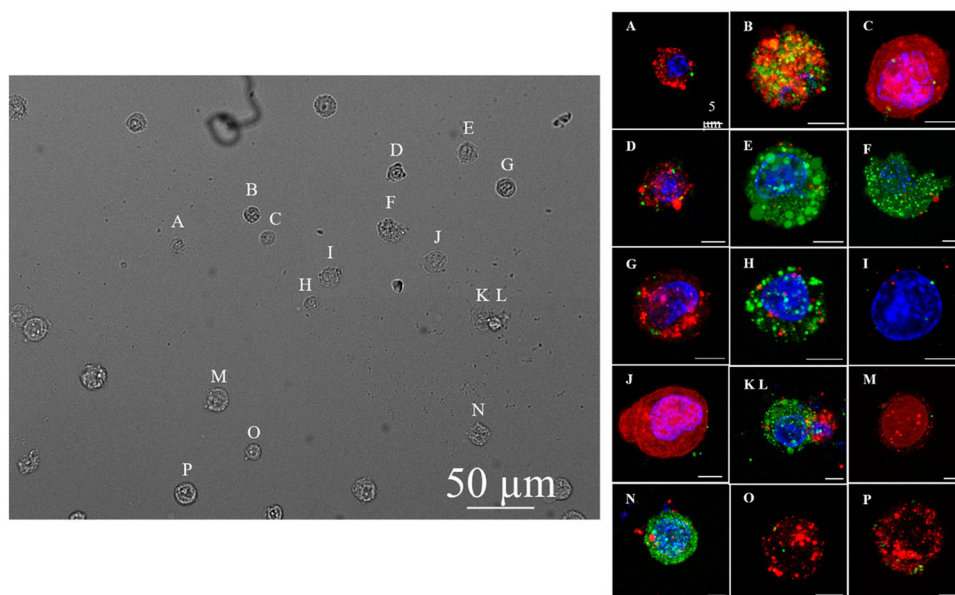


FIGURE 6 Widefield examination to detail uptake of extracellular vesicles (EVs) by Chinese hamster ovary (CHO) cells. Widefield study for CHO EV exchange quantification in a coculture of GFP (green) CHO and RFP (red) CHO cells at 24 h (DAPI, blue). All cells in the widefield image were positive for GFP and RFP demonstrating the widespread exchange of CHO EVs in culture

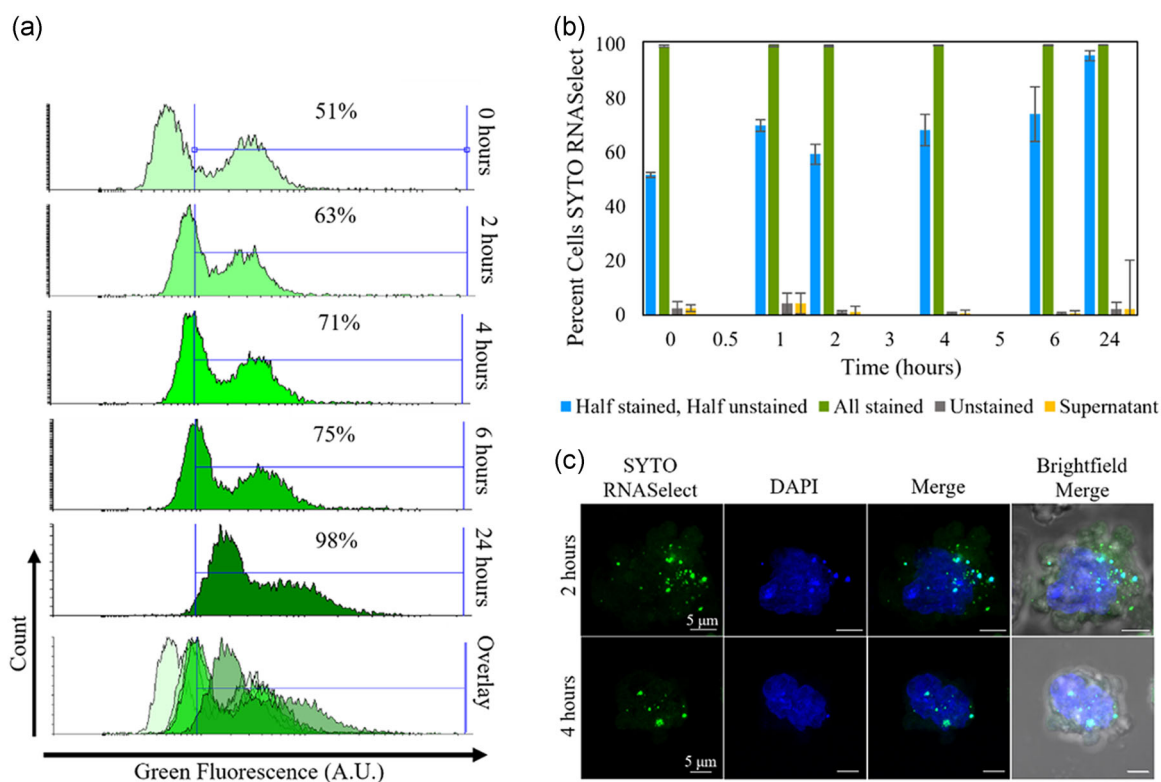


FIGURE 7 Exchange of cellular RNA between Chinese hamster ovary (CHO) cells through dynamic extracellular vesicle (EV) formation and uptake. CHO coculture with half unstained cells (2×10^6 cells) and half SYTO RNaselect stained cells (2×10^6 cells) in $100 \mu\text{l}$ for the first hour to enhance contact between cells and EVs before the volume is increased to 1 ml for 24 h. (a) Flow cytometry of the coculture over 24 h. At 0 h, there are two populations, unstained cells (left peak) and SYTO RNaselect stained cells (right peak), and 51% of the coculture population are green fluorescent. Green fluorescent intensity in the coculture increases over 24 h, where 98% of cells green fluorescent. (b) Cocultures with half SYTO RNaselect stained cells and half unstained cells increase in percent of cells positive for SYTO RNaselect over 24 h evaluated via flow cytometry. Control cultures with all cells SYTO RNaselect stained and cultures with all cells unstained (three biological replicates). (c) Unstained culture of cells were cocultured with EVs isolated from a SYTO RNaselect culture for 2 and 4 h evaluated via confocal microscopy. Observed uptake of stained EVs by unstained cells demonstrates the massive exchange of RNA material between cells in culture via EVs

replicates over the course of 24 h. Figure 7b captures the average shift in the percent of cells positive for the SYTO RNaselect stained cells among the replicate cultures. Cocultures starting with half SYTO RNaselect cells and half unstained cells increased the number of SYTO RNaselect positive cells from 52% at 0 h to 96% at 24 h. Additionally, a culture of 4×10^6 unstained cells were grown in the supernatant of the final wash step of SYTO RNaselect stained cells. This culture was included to evaluate if the shift in SYTO RNaselect positive cells was due to excess stain in the media after the several washing steps in the staining protocol and it was concluded that excess dye was not the cause of the increase in SYTO RNaselect positive cells in cocultures. We conclude that the shift in the percent of SYTO RNaselect cells was due to the exchange of EVs from stained cells to unstained cells and this was supported by confocal microscopy.

Confocal microscopy of the RNA-stained cocultures identified individual CHO EVs within unstained CHO cells at 24 h (Figure 7c). Similar to the fluorescent protein studies, confocal microscopy can only capture intact EVs taken up by a cell at a given timepoint and does not capture the total number of EVs taken up by a cell throughout the lifespan of the culture. The exchange of EVs observed in the coculture of unstained and SYTO RNaselect stained cells mirrored the levels of exchange observed with confocal microscopy using fluorescent proteins (Figures 4–6) where at 24 h of coculture, 98% of cells were positive for the SYTO RNaselect stain. We hypothesize the high levels of EV exchange in coculture that was

observed on flow cytometry with the SYTO RNaselect stained cells, but not with the protein stains or fluorescent proteins (data not shown), was due to the large abundance of RNA (notably rRNA) in the EVs and the brighter fluorescence intensity of the RNA stain.

3.4 | Dynamic exchange of protein material in the human CHRF cell line and primary human hematopoietic stem cells

Widespread exchange of EVs in culture was also observed in the human CHRF-288-11 (CHRF) megakaryoblastic cell line and in human CD34⁺ Hematopoietic Stem & Progenitor Cells (HSPCs). EmGFP CHRF cells were cocultured with miRFP CHRF cells for 48 h. Similar to the CHO cocultures, EmGFP CHRF cells produced EmGFP CHRF EVs and miRFP CHRF cells produced miRFP CHRF EVs and the exchange of fluorescent EVs was observed. Representative images of CHRF cocultures demonstrate the widespread exchange of EVs in cultures (Figure 8) and numerous taken up EVs were taken up by the target cells. We estimate that EVs exchange was observed in approximately 80% of CHRF cells in coculture with confocal microscopy.

Primary human HSPCs were also examined aiming to demonstrate the generality of cellular material exchange between cells in culture via EVs. It was previously shown that CHRF EVs are taken up by cultured HSPCs (Kao & Papoutsakis, 2018). Human HSPCs from

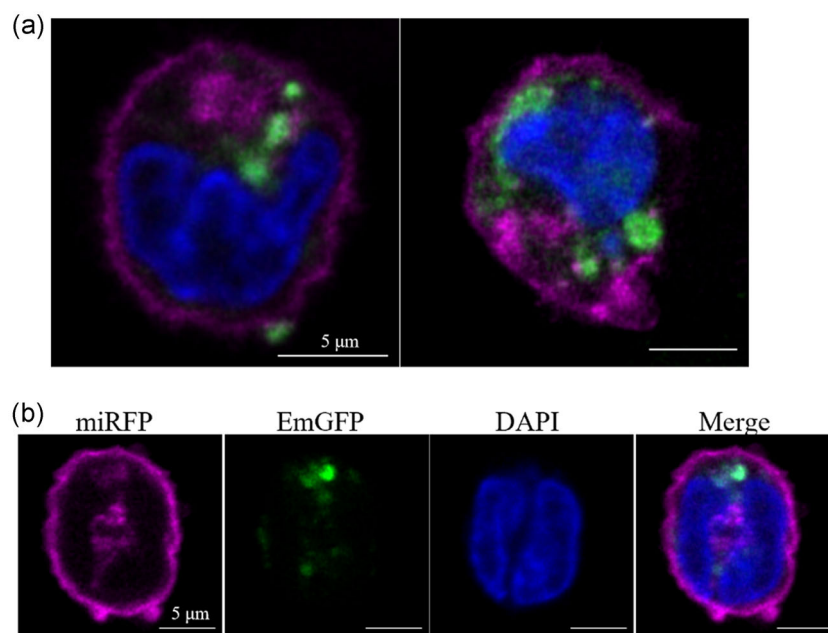


FIGURE 8 Visualization of extracellular vesicle (EV) exchange between CHRF cells in culture. Confocal images of individual cells at the 24-h time point of a coculture of EmGFP CHRF (green) and miRFP CHRF (magenta) cells. DAPI (blue) is for staining the nuclei. EmGFP CHRF derived EVs are taken up by miRFP CHRF cells. CHRF EVs are observed at the periphery and center of the CHRF cell. (a) In maximum intensity projection confocal images, distinct EmGFP CHRF EV signal is detected in the cytoplasm of miRFP CHRF cells. Fluorescent signal from EVs were both concentrated and diffuse suggesting EVs within the cell are both intact and unloading cargo into the cell. (b) A maximum intensity projection confocal image of a miRFP CHRF cell with both individual fluorescent channels and a merged fluorescent channel. The green channel representing EmGFP CHRF EVs shows intact EVs colocalizing to the cell cytoplasm

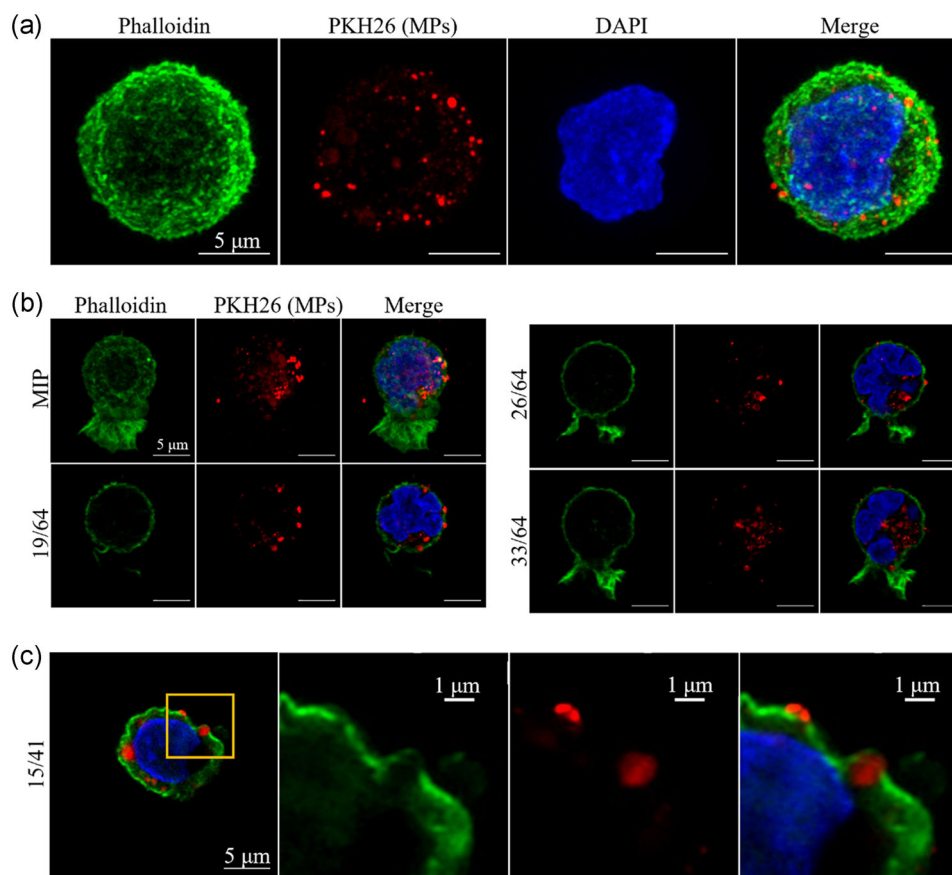


FIGURE 9 Uptake of CHRF microparticles (MPs) by human HSPCs. Day 3 HSPCs (actin stained with phalloidin, green) were cocultured with CHRF MPs stained with the lipophilic membrane stain PKH26 (red). Confocal images of individual cells at (a) 24 h and (b,c) 48 h (nucleus stained with DAPI, blue). (a) Maximum intensity projection (MIP) image of a single HSPC and PKH26 stained CHRF EVs inside the cell. (b) MIP image of a single HSPC containing stained CHRF EVs at the different z-planes of the HSPC. CHRF EVs are observed at the periphery and center of the cell. (c) CHRF EVs are internalized by an HSPC and zoomed-in images of a CHRF MP shortly after uptake at the HSPC membrane

Days 3 or 5 of standard HSPC cultures (Kao & Papoutsakis, 2018) were cocultured with either isolated EmGFP CHRF MPs or isolated CHRF MPs stained with the lipophilic membrane stain PKH26 at a ratio of 100 MPs per cell. The HSPC cell membrane was visualized with the green fluorescent actin stain phalloidin and the nucleus was stained with DAPI. Coculture samples of the HSPCs and isolated CHRF EVs were collected at 24 and 48 h and analyzed with confocal microscopy (Figure 9). CHRF MPs were readily taken up by Days 3 and 5 HSPCs in coculture. A representative MIP image of an HSPC from the coculture (Figure 9a) demonstrates the total number of intact CHRF MPs at the cell surface and taken up by the cell. HSPCs were motile in culture and HSPCs with uropod structures were observed (Figure 9b). The uropod structure has been reported to be an important mediator and preferred interaction site of EV uptake in HSPCs (Jiang et al., 2017).

Early CHRF EV uptake by HSPCs demonstrate the imbedding of the MPs in the cell membrane (Figure 9c). The cell membrane (actin stain phalloidin, green) wraps around the intact PKH26 stained CHRF EV provides further visual evidence for HSPCs endocytosis of EVs (Jiang et al., 2017). From our observations, we estimate

approximately 90% of HSPCs were taking up labeled CHRF EVs as 88% of cells (18 total cells) imaged at 24 h had dual fluorescence.

Cocultures with CHO cells, CHRF cells, and HSPCs demonstrate the widespread phenomena of EV exchange and uptake and represent a mechanism for large amounts of protein and RNA exchange between cells in culture that appears to be independent of cell type.

4 | DISCUSSION

The cell surface morphology of CHO cells observed via SEM (Figure 2), supports the previously underappreciated concept that CHO cells are in a constant process of producing and taking up CHO EVs generated in the culture. We hypothesize this dynamic EV exchange process allows a culture of suspension cells to share large quantities of protein and RNA to regulate cellular processes as a whole culture instead of as individual cells.

The simple EV generation and consumption model we present provides insight into an approximate amount of EVs the CHO cells are producing and taking up each day in culture. To our knowledge,

this is the first reported EV production estimates. The proposed simple model (Equation 1) for EV production and uptake provides a method that can be applied to other experimental data sets to estimate EV production of different cultured cells and culture conditions. Other studies have reported the number of EVs in the media on a per cell basis as a frame of reference for estimating EV production (Soo et al., 2012), however, calculating the number of EVs accumulated in the media neglects EV uptake and EV accumulation and is not the same as the rate of production. Our data (Figure S1d) show similar values for EVs per cell: a range of approximately 50–1000 EVs per cell.

With a fixed number of cells and EVs, EV uptake by cells is quite fast peaking within 1–2 h as shown for example by data in our work (Jiang et al., 2017). Thus, to estimate k_2E and k_2 , one could incubate known number of cells with different concentrations of labeled EVs over 4–6 h and count the number of labeled EVs that have been taken up by the cells. Estimating the number of EVs a cell takes up can be used to estimate the total amount of protein and RNA material exchanged between cells under different culture conditions. Additionally, when utilizing EVs to deliver specific cargo molecules, estimation of EV uptake rates allows for better designs in EV delivery strategies. The proposed model of Equation (1) is a starting point for estimating EV production and uptake and more comprehensive models can more accurately capture the dynamics of production and uptake throughout culture in different growth phases and culture conditions.

While in this study we focused on capturing the production and uptake of EVs in culture to better understand protein and RNA exchange between cells via EVs, future studies will focus on identifying the specific cargo natively within CHO EVs. In a recent study, Keysberg et al. (2021) completed proteomic and noncoding RNA (microRNA and PIWI-interacting RNA) analysis of CHO exosomes from lab-scale bioreactors, providing insight into the specific proteins and RNAs transferred via EVs we may have observed in cocultures.

The exchange of EVs in a culture can be studied with lipophilic protein stains and with fluorescently expressing cell lines. Cocultures with half of the cells in culture expressing RFP and the other half expressing GFP as well as cocultures with half the cells in culture stained with CellTracker Deep Red and the other half stained with CFDA-SE both result in exchange of proteins through EVs. Confocal microscopy best captured the fluorescent protein exchange to evaluate the massive exchange of EVs and correlative confocal/SEM studies identified specific uptake events in individual cells. We observed distinct EVs bound to the cell membrane and were interacting with microvilli, suggesting a potentially important role of microvilli in CHO EV uptake. In both fluorescent protein cocultures, the majority of cells observed in coculture contained both fluorescent signals, demonstrating the massive exchange of EVs in CHO cultures.

Fluorescent protein-expressing cells lines, such as the RFP and GFP expressing CHO cell lines used here, address concerns of decaying protein stains as cells in culture divide (Wang et al., 2005). Additionally, fluorescent protein-expressing cell lines offer improved visualization of EVs on confocal microscopy over lipophilic protein stains. In the situation where fluorescently expressing cell lines are not

available, such as primary cell cultures, lipophilic protein stains were shown to be a sufficient tool for visualizing and quantifying the extent of EV exchange in culture. While either approach is suitable when using fluorescent microscopy, flow-cytometric analysis remains a problem with either approach for lack of sensitivity of the fluorescent material associated with the process of EV uptake and dissolution into cells. Indeed, our findings demonstrate vast differences in quantifying EV uptake between flow cytometry and confocal microscopy with the later having greater sensitivity for EV detection via fluorescent proteins. Due to this profound underestimation of EV exchange via fluorescent proteins in culture with flow cytometry, confocal microscopy was the preferred method for observing and quantifying EV uptake and notably the associated exchange of proteins.

Fluorescent RNA-specific stains are an alternative method for tracking the uptake of EVs in culture (Li et al., 2014; O'Brien et al., 2020). CHO cells stained with an RNA-specific stain produced EVs containing fluorescent RNA content that was observed transferred between cells. Evaluating EV exchange with stained RNA may be advantageous due to the abundance of RNAs natively found within EVs. RNA-specific stains were easier to detect with flow cytometry compared to protein stains and fluorescent proteins. In a coculture with half the cells unstained and half the cells RNA stained, after 6 h of coculture, 75% of the cells contained the fluorescent RNA stain via CHO EVs. At 24 h, 98% of cells in the coculture were positive for the RNA stain. Individual EVs taken up by unstained cells in coculture were observed with confocal microscopy to confirm the unstained cells contained fluorescent CHO EVs. Flow cytometry analysis of EVs via stained RNA provides quantitative evidence for the vast extent of EV exchange in culture and the kinetics of EV production and uptake in culture. To summarize, in CHO cultures the continuous production and uptake of EVs in culture results in the delivery of proteins and RNA (including regulatory small RNAs but also mRNAs) from other cells throughout the culture duration. The potential impact of this large-scale exchange may be an extensive cytoplasm homogenization of the cell population in culture.

Prior literature has investigated the relationship between cancer cells and stem cells and the transfer of regulatory RNAs via EVs to progress or inhibit tumor growth (Adamo et al., 2019; Fonsato et al., 2012; Lee et al., 2013; Sandiford et al., 2021; Zhou et al., 2019). The ability of tumor cells and stem cells to communicate throughout the body and in culture presents interesting questions on the effects of how cancer-cell derived EVs and stem-cell EVs can influence the regulation of cell functions. These findings combined with the widespread exchange in CHO cells suggest widespread EV exchange is a universal occurrence in eukaryotic cells and cells rely, at least in part, on EVs from other cells to regulate cellular functions.

Our data support the concept that EVs distribute large quantities of mRNA, regulatory RNAs such as microRNAs, and proteins to all cells in culture or in near proximity in tissues. There are several implications of this phenomenon. One potential scenario could take place when a spontaneous mutation arises that could affect cell viability and proliferation, such as early induction of apoptosis. This could affect the culture in a detrimental way such as in the

production of a recombinant protein. The microRNA cluster miR-297-669 has been hypothesized to stimulate apoptosis with nutrient depletion (Druz et al., 2011) and miR-466h from this cluster has been studied as it targets antiapoptotic genes (Druz et al., 2011, 2012). If a clone arises in a culture that enters apoptosis early and is highly enriched in miR-466h, EVs produced by this cell likely will be enriched in miR-466h. As EVs enriched in miR-466h are circulated in culture and taken up, miR-466h may suppress antiapoptotic genes and cause the mutated clone to promote apoptosis in the whole culture. Other scenarios could involve mutations in miRNAs that are positively or negatively affect the expression of native and engineered proteins (Fischer et al., 2015; Kelly et al., 2015; Loh et al., 2014). As well as scenarios involving mutations of RNAs that control genome stability (Chan et al., 2014), such as mutations of the RNA exosome complex (de Andrade et al., 2020), whose role remains poorly understood.

In physiologically relevant studies, extracellular vesicles derived from cells with high-metastatic cancer cells have been observed to promote metastasis in cells with low-metastatic potential both in vitro and in vivo (Yang et al., 2020). As observed in this study, EVs from the acute megakaryoblastic leukemia cell line CHR-288-11 were readily taken up by HSPCs in coculture, suggesting cancer cells can influence the expression of stem cells. Studies have reported on the effects of cancer cell-derived EVs on stem cells (Chin & Wang, 2016; Daßler-Plenker et al., 2020; Henrich et al., 2020) and in this study, we were able to observe the large extent of cancer-derived EVs uptake by HSPCs.

ACKNOWLEDGMENTS

We thank Sylvain Le Marchand and Deborah Powell and members of the Delaware Biotechnology Institute's Bio-Imaging Center for assistance with correlative confocal and scanning electron microscopy. Microscopy equipment was acquired with a shared instrument grants (S10 OD16361, S10 OD025165) and the Delaware INBRE Grant P20 GM103446 and access was supported by grants from the NIH-NIGMS (P20 GM103446), the NSF (IIA-1301765), and the State of Delaware. We thank Professor Kelvin Lee and Nathaniel Hamaker for the GFP expressing CHO cell line. We thank the Advanced Mammalian Biomanufacturing Innovation Center (AMBIC, NSF Grant1624698), MilliporeSigma, and Sartorius for funding.

CONFLICT OF INTERESTS

The authors declare no conflict of interest.

AUTHOR CONTRIBUTIONS

Eleftherios T. Papoutsakis and Jessica Belliveau designed the study and analyzed the data; Jessica Belliveau carried out the experiments. Eleftherios T. Papoutsakis and Jessica Belliveau wrote the manuscript.

DATA AVAILABILITY STATEMENT

The data used to support the findings of this study are available from the corresponding author upon request.

ORCID

Jessica Belliveau  <http://orcid.org/0000-0003-3466-6428>

Eleftherios T. Papoutsakis  <http://orcid.org/0000-0002-1077-1277>

REFERENCES

- Adamo, A., Dal Collo, G., Bazzoni, R., & Krampera, M. (2019). Role of mesenchymal stromal cell-derived extracellular vesicles in tumour microenvironment. *Biochimica et Biophysica Acta (BBA)—Reviews on Cancer*, 1871(1), 192–198. <https://doi.org/10.1016/j.bbcan.2018.12.001>
- Boudreau, L. H., Duchez, A.-C., Cloutier, N., Soulet, D., Martin, N., Bollinger, J., Paré, A., Rousseau, M., Naika, G. S., Lévesque, T., Laflamme, C., Marcoux, G., Lambeau, G., Farndale, R. W., Pouliot, M., Hamzeh-Cognasse, H., Cognasse, F., Garraud, O., Nigrovic, P. A., ... Boilard, E. (2014). Platelets release mitochondria serving as substrate for bactericidal group IIA-secreted phospholipase A2 to promote inflammation. *Blood*, 124(14), 2173–2183. <https://doi.org/10.1182/blood-2014-05-573543>
- Chan, Y. A., Hieter, P., & Stirling, P. C. (2014). Mechanisms of genome instability induced by RNA-processing defects. *Trends in Genetics*, 30(6), 245–253. <https://doi.org/10.1016/j.tig.2014.03.005>
- Charubin, K., Modla, S., Caplan, J. L., & Papoutsakis, E. T. (2020). Interspecies microbial fusion and large-scale exchange of cytoplasmic proteins and RNA in a syntrophic clostridium coculture. *mBio*, 11(5), e02030-20. <https://doi.org/10.1128/mBio.02030-20>
- Chin, A. R., & Wang, S. E. (2016). Cancer-derived extracellular vesicles: The 'soil conditioner' in breast cancer metastasis? *Cancer and Metastasis Reviews*, 35(4), 669–676. <https://doi.org/10.1007/s10555-016-9639-8>
- Daßler-Plenker, J., Küttner, V., & Egeblad, M. (2020). Communication in tiny packages: Exosomes as means of tumor-stroma communication. *Biochimica et Biophysica Acta (BBA)—Reviews on Cancer*, 1873(2), 188340. <https://doi.org/10.1016/j.bbcan.2020.188340>
- de Andrade, I. F., Mehta, C., & Bresnick, E. H. (2020). Post-transcriptional control of cellular differentiation by the RNA exosome complex. *Nucleic Acids Research*, 48(21), 11913–11928. <https://doi.org/10.1093/nar/gkaa883>
- De Chaumont, F., Dallongeville, S., Chenouard, N., Hervé, N., Pop, S., Provoost, T., Meas-Yedid, V., Pankajakshan, P., Lecomte, T., Le Montagner, Y., Lagache, T., Dufour, A., & Olivo-Marin, J. C. (2012). Icy: An open bioimage informatics platform for extended reproducible research. *Nature Methods*, 9(7), 690–696. <https://doi.org/10.1038/nmeth.2075>
- de Jong, O. G., Verhaar, M. C., Chen, Y., Vader, P., Gremmels, H., Posthuma, G., Schiffelers, R. M., Gucek, M., & van Balkom, B. W. (2012). Cellular stress conditions are reflected in the protein and RNA content of endothelial cell-derived exosomes. *Journal of Extracellular Vesicles*, 1(1), 18396. <https://doi.org/10.3402/jev.v1i0.18396>
- Di Trapani, M., Bassi, G., Midolo, M., Gatti, A., Takam Kamga, P., Cassaro, A., Carusone, R., Adamo, A., & Krampera, M. (2016). Differential and transferable modulatory effects of mesenchymal stromal cell-derived extracellular vesicles on T, B and NK cell functions. *Scientific Reports*, 6(1), 24120. <https://doi.org/10.1038/srep24120>
- Druz, A., Betenbaugh, M., & Shiloach, J. (2012). Glucose depletion activates mmu-miR-466h-5p expression through oxidative stress and inhibition of histone deacetylation. *Nucleic Acids Research*, 40(15), 7291–7302. <https://doi.org/10.1093/nar/gks452>
- Druz, A., Chu, C., Majors, B., Santuary, R., Betenbaugh, M., & Shiloach, J. (2011). A novel microRNA mmu-miR-466h affects apoptosis regulation in mammalian cells. *Biotechnology and Bioengineering*, 108(7), 1651–1661. <https://doi.org/10.1002/bit.23092>

- Escobar, C., Kao, C.-Y., Das, S., & Papoutsakis, E. T. (2020). Human megakaryocytic microparticles induce de novo platelet biogenesis in a wild-type murine model. *Blood Advances*, 4(5), 804–814. <https://doi.org/10.1182/bloodadvances.2019000753>
- Fischer, S., Paul, A. J., Wagner, A., Mathias, S., Geiss, M., Schandock, F., Domnowski, M., Zimmermann, J., Handrick, R., Hesse, F., & Otte, K. (2015). miR-2861 as novel HDAC5 inhibitor in CHO cells enhances productivity while maintaining product quality. *Biotechnology and Bioengineering*, 112(10), 2142–2153. <https://doi.org/10.1002/bit.25626>
- Fonsato, V., Collino, F., Herrera, M. B., Cavallari, C., Deregibus, M. C., Cisterna, B., Bruno, S., Romagnoli, R., Salizzoni, M., Tetta, C., & Camussi, G. (2012). Human liver stem cell-derived microvesicles inhibit hepatoma growth in SCID mice by delivering antitumor microRNAs. *Stem Cells*, 30(9), 1985–1998. <https://doi.org/10.1002/stem.1161>
- Fuhrken, P. G., Apostolidis, P. A., Lindsey, S., Miller, W. M., & Papoutsakis, E. T. (2008). Tumor suppressor protein p53 regulates megakaryocytic polyploidization and apoptosis. *Journal of Biological Chemistry (Baltimore, MD)*, 283(23), 15589–15600. <https://doi.org/10.1074/jbc.M801923200>
- García-Contreras, M., Shah, S. H., Tamayo, A., Robbins, P. D., Golberg, R. B., Mendez, A. J., & Ricordi, C. (2017). Plasma-derived exosome characterization reveals a distinct microRNA signature in long duration Type 1 diabetes. *Scientific Reports*, 7(1), 5998. <https://doi.org/10.1038/s41598-017-05787-y>
- Han, S., & Rhee, W. J. (2018). Inhibition of apoptosis using exosomes in Chinese hamster ovary cell culture. *Biotechnology and Bioengineering*, 115(5), 1331–1339. <https://doi.org/10.1002/bit.26549>
- Henrich, S. E., McMahon, K. M., Plebanek, M. P., Calvert, A. E., Feliciano, T. J., Parrish, S., Tavora, F., Mega, A., De Souza, A., Carneiro, B. A., & Thaxton, C. S. (2020). Prostate cancer extracellular vesicles mediate intercellular communication with bone marrow cells and promote metastasis in a cholesterol-dependent manner. *Journal of Extracellular Vesicles*, 10(2), e12042. <https://doi.org/10.1002/jev2.12042>
- Jeppesen, D. K., Fenix, A. M., Franklin, J. L., Higginbotham, J. N., Zhang, Q., Zimmerman, L. J., Liebler, D. C., Ping, J., Liu, Q., Evans, R., Fissel, W. H., Patton, J. G., Rome, L. H., Burnette, D. T., & Coffey, R. J. (2019). Reassessment of exosome composition. *Cell*, 177(2), 428–445. <https://doi.org/10.1016/j.cell.2019.02.029>
- Jiang, J. L., Kao, C. Y., & Papoutsakis, E. T. (2017). How do megakaryocytic microparticles target and deliver cargo to alter the fate of hematopoietic stem cells? *Journal of Controlled Release*, 247, 1–18. <https://doi.org/10.1016/j.jconrel.2016.12.021>
- Jiang, J. L., Woulfe, D. S., & Papoutsakis, E. T. (2014). Shear enhances thrombopoiesis and formation of microparticles that induce megakaryocytic differentiation of stem cells. *Blood*, 124(13), 2094–2103. <https://doi.org/10.1182/blood-2014-01-547927>
- Kao, C.-Y., & Papoutsakis, E. T. (2018). Engineering human megakaryocytic microparticles for targeted delivery of nucleic acids to hematopoietic stem and progenitor cells. *Science Advances*, 4(11), eaau6762. <https://doi.org/10.1126/sciadv.aau6762>
- Kao, C.-Y., & Papoutsakis, E. T. (2019). Extracellular vesicles: Exosomes, microparticles, their parts, and their targets to enable their biomanufacturing and clinical applications. *Current Opinion in Biotechnology*, 60, 89–98. <https://doi.org/10.1016/j.copbio.2019.01.005>
- Kelly, P. S., Gallagher, C., Clynes, M., & Barron, N. (2015). Conserved microRNA function as a basis for Chinese hamster ovary cell engineering. *Biotechnology Letters*, 37(4), 787–798. <https://doi.org/10.1007/s10529-014-1751-7>
- Kesimer, M., & Gupta, R. (2015). Physical characterization and profiling of airway epithelial derived exosomes using light scattering. *Methods*, 87, 59–63. <https://doi.org/10.1016/j.ymeth.2015.03.013>
- Keysberg, C., Hertel, O., Schelletter, L., Busche, T., Sochart, C., Kalinowski, J., Hoffrogge, R., Otte, K., & Noll, T. (2021). Exploring the molecular content of CHO exosomes during bioprocessing. *Applied Microbiology and Biotechnology*, 105(9), 3673–3689. <https://doi.org/10.1007/s00253-021-11309-8>
- Lee, J.-K., Park, S.-R., Jung, B.-K., Jeon, Y.-K., Lee, Y.-S., Kim, M.-K., Kim, Y. G., Jang, J. Y., & Kim, C. W. (2013). Exosomes derived from mesenchymal stem cells suppress angiogenesis by down-regulating VEGF expression in breast cancer cells. *PLoS ONE*, 8(12), e84256. <https://doi.org/10.1371/journal.pone.0084256>
- Li, M., Zeringer, E., Barta, T., Schageman, J., Cheng, A., & Vlassov, A. V. (2014). Analysis of the RNA content of the exosomes derived from blood serum and urine and its potential as biomarkers. *Philosophical Transactions of the Royal Society, B: Biological Sciences*, 369(1652), 20130502. <https://doi.org/10.1098/rstb.2013.0502>
- Loh, W. P., Loo, B., Zhou, L. H., Zhang, P. Q., Lee, D. Y., Yang, Y. S., & Lam, K. P. (2014). Overexpression of microRNAs enhances recombinant protein production in Chinese hamster ovary cells. *Biotechnology Journal*, 9(9), 1140–1151. <https://doi.org/10.1002/biot.201400050>
- Midekessa, G., Godakumara, K., Ord, J., Viil, J., Lättekivi, F., Dissanayake, K., Kopanchuk, S., Rinken, A., Andronowska, A., Bhattacharjee, S., Rinken, T., & Fazeli, A. (2020). Zeta potential of extracellular vesicles: Toward understanding the attributes that determine colloidal stability. *ACS Omega*, 5(27), 16701–16710. <https://doi.org/10.1021/acsomega.0c01582>
- Nassar, W., El-Ansary, M., Sabry, D., Mostafa, M. A., Fayad, T., Kotb, E., Temraz, M., Saad, A. N., Essa, W., & Adel, H. (2016). Umbilical cord mesenchymal stem cells derived extracellular vesicles can safely ameliorate the progression of chronic kidney diseases. *Biomaterials Research*, 20, 21. <https://doi.org/10.1186/s40824-016-0068-0>
- Njock, M. S., Cheng, H. S., Dang, L. T., Nazari-Jahantigh, M., Lau, A. C., Boudreau, E., Roufaiel, M., Cybulsky, M. I., Schober, A., & Fish, J. E. (2015). Endothelial cells suppress monocyte activation through secretion of extracellular vesicles containing antiinflammatory microRNAs. *Blood*, 125(20), 3202–3212. <https://doi.org/10.1182/blood-2014-11-611046>
- O'Brien, K., Breyne, K., Ughetto, S., Laurent, L. C., & Breakefield, X. O. (2020). RNA delivery by extracellular vesicles in mammalian cells and its applications. *Nature Reviews Molecular Cell Biology*, 21(10), 585–606. <https://doi.org/10.1038/s41580-020-0251-y>
- Paul-Gilloteaux, P., Heiligenstein, X., Belle, M., Domart, M. -C., Larjani, B., Collinson, L., Raposo, G., & Salameiro, J. (2017). eC-CLEM: Flexible multidimensional registration software for correlative microscopies. *Nature Methods*, 14(2), 102–103. <https://doi.org/10.1038/nmeth.4170>
- Raposo, G., & Stoorvogel, W. (2013). Extracellular vesicles: Exosomes, microvesicles, and friends. *Journal of Cell Biology (New York, NY)*, 200(4), 373–383. <https://doi.org/10.1083/jcb.201211138>
- Sandiford, O. A., Donnelly, R. J., El-Far, M. H., Burgmeyer, L. M., Sinha, G., Pamarthi, S. H., Sherman, L. S., Ferrer, A. I., DeVore, D. E., Patel, S. A., Naaldijk, Y., Alonso, S., Barak, P., Bryan, M., Ponzio, N. M., Narayanan, R., Etchegaray, J. P., Kumar, R., & Rameshwar, P. (2021). Mesenchymal stem cell-secreted extracellular vesicles instruct stepwise dedifferentiation of breast cancer cells into dormancy at the bone marrow perivascular region. *Cancer Research*, 81(6), 1567–1582. <https://doi.org/10.1158/0008-5472.can-20-2434>
- Sansone, P., Savini, C., Kurelac, I., Chang, Q., Amato, L. B., Strillacci, A., Stepanova, A., Iommarini, L., Mastroleo, C., Daly, L., Galkin, A., Thakur, B. K., Soplop, N., Uryu, K., Hoshino, A., Norton, L., Bonafé, M., Cricca, M., Gasparre, G., ... Bromberg, J. (2017). Packaging and transfer of mitochondrial DNA via exosomes regulate escape from dormancy in hormonal therapy-resistant breast cancer. *Proceedings of the National Academy of Sciences of the United States of America*, 114(43), E9066–E9075. <https://doi.org/10.1073/pnas.1704862114>

- Seras-Franzoso, J., Díaz-Riascos, Z. V., Corchero, J. L., González, P., García-Aranda, N., Mandaña, M., Riera, R., Boullosa, A., Mancilla, S., Grayston, A., Moltó-Abad, M., García-Fruitós, E., Mendoza, R., Pintos-Morell, G., Albertazzi, L., Rosell, A., Casas, J., Villaverde, A., Schwartz, S., & Abasolo, I. (2021). Extracellular vesicles from recombinant cell factories improve the activity and efficacy of enzymes defective in lysosomal storage disorders. *Journal of Extracellular Vesicles*, 10(5), e12058. <https://doi.org/10.1002/jev2.12058>
- Sokolova, V., Ludwig, A. K., Hornung, S., Rotan, O., Horn, P. A., Epple, M., & Giebel, B. (2011). Characterisation of exosomes derived from human cells by nanoparticle tracking analysis and scanning electron microscopy. *Colloids and Surfaces B, Biointerfaces*, 87(1), 146–150. <https://doi.org/10.1016/j.colsurfb.2011.05.013>
- Soo, C. Y., Song, Y., Zheng, Y., Campbell, E. C., Riches, A. C., Gunn-Moore, F., & Powis, S. J. (2012). Nanoparticle tracking analysis monitors microvesicle and exosome secretion from immune cells. *Immunology*, 136(2), 192–197. <https://doi.org/10.1111/j.1365-2567.2012.03569.x>
- Wang, X.-Q., Duan, X.-M., Liu, L.-H., Fang, Y.-Q., & Tan, Y. (2005). Carboxyfluorescein diacetate succinimidyl ester fluorescent dye for cell labeling. *Acta Biochimica et Biophysica Sinica*, 37(6), 379–385. <https://doi.org/10.1111/j.1745-7270.2005.00051.x>
- Yang, B., Feng, X., Liu, H., Tong, R., Wu, J., Li, C., Yu, H., Chen, Y., Cheng, Q., Chen, J., Cai, X., Wu, W., Lu, Y., Hu, J., Liang, K., Lv, Z., Wu, J., & Zheng, S. (2020). High-metastatic cancer cells derived exosomal miR92a-3p promotes epithelial-mesenchymal transition

and metastasis of low-metastatic cancer cells by regulating PTEN/Akt pathway in hepatocellular carcinoma. *Oncogene*, 39(42), 6529–6543. <https://doi.org/10.1038/s41388-020-01450-5>

- Zhou, X., Li, T., Chen, Y., Zhang, N., Wang, P., Liang, Y., Long, M., Liu, H., Mao, J., Liu, Q., Sun, X., & Chen, H. (2019). Mesenchymal stem cell-derived extracellular vesicles promote the in vitro proliferation and migration of breast cancer cells through the activation of the ERK pathway. *International Journal of Oncology*, 54, 1843–1852. <https://doi.org/10.3892/ijo.2019.4747>

SUPPORTING INFORMATION

Additional supporting information may be found in the online version of the article at the publisher's website.

How to cite this article: Belliveau, J., & Papoutsakis, E. T. (2022). Extracellular vesicles facilitate large-scale dynamic exchange of proteins and RNA among cultured Chinese hamster ovary and human cells. *Biotechnology and Bioengineering*, 119, 1222–1238. <https://doi.org/10.1002/bit.28053>